Eur. Phys. J. D **38**, 445–454 (2006)
DOI: 10.1140/epjd/e2006-00052-0

THE EUROPEAN PHYSICAL JOURNAL D

Relaxation of spin polarized ^{3}He by magnetized ferromagnetic contaminants

Part III

J. Schmiedeskamp[1,a], H.-J. Elmers[1], W. Heil[1,b], E.W. Otten[1,c], Yu. Sobolev[1,d], W. Kilian[2], H. Rinneberg[2], T. Sander-Thömmes[2], F. Seifert[2], and J. Zimmer[3]

[1] Institut für Physik, 55099 Mainz, Germany
[2] Physikalisch-Technische Bundesanstalt, 10587 Berlin, Germany
[3] Schott AG Mainz, Germany

Received 26 August 2005 / Received in final form 19 December 2005
Published online 14 March 2006 –

Abstract. In the first in a series of three papers on wall relaxation of spin polarized ^{3}He we have reported on a breakdown of relaxation times which is observed after exposing the ^{3}He containing glass cells to a strong magnetizing field. In this third paper we give a quantitative analysis of this phenomenon, based on magnetic signal detection by means of SQUIDs, on the pressure dependence of relaxation times in magnetized cells, as well as on Monte Carlo simulations of ^{3}He-relaxation in a macroscopic dipole field. Our analysis allows to identify the contaminants as being aggregates of dust-like Fe_3O_4 particles (magnetite) with a radius $R \approx 10$ μm and a remanent magnetic moment of the order of $m \approx O(10^{-10}$ A m$^2)$. The particles are located at or close to the inner glass surface.

PACS. 33.25.+k Nuclear resonance and relaxation – 34.50.Dy Interactions of atoms and molecules with surfaces; photon and electron emission; neutralization of ions – 67.65.+z Spin-polarized hydrogen and helium

1 Introduction

The first hint that agents other than paramagnetic centres may contribute to relaxation of ^{3}He spins at glass walls can already be found in an early paper by Fitzsimmons et al. [1]. They have observed a magnetic field dependence of relaxation times T_1 of ^{3}He contained in cells from borosilicate (Pyrex) or aluminosilicate glass. Recently Jacob et al. [2,3] have substantiated these findings by systematically studying T_1 in various types of Rb coated cells which were exposed to low and high magnetic fields. They clearly demonstrate that the relaxation rates show hysteresis and remanence as function of the applied field. They conclude that ferromagnetic species at or near to the glass surface must be present which enhance relaxation if magnetized. Since they did not find this effect in bare glass cells, they concluded that small iron particles had been dragged in along with the metallic rubidium filled into the cell. Hence we were taken by surprise to find that our bare 1.1 litre cells — blown directly from melts of iron-free aluminosilicate glasses — got magnetized as well when exposed to the 1.5 T field of a MR tomograph during administering hyperpolarized ^{3}He to patients. Their remanent magnetism caused a breakdown of relaxation times down to a minimum of $\langle T_{1,min}\rangle = 17$ h averaged over 31 cells in use. In a properly demagnetized state, however, the same sample attains a very satisfactory average of relaxation times as high as $\langle T_{1,max}\rangle = 150$ h. This phenomenon has been described in the first paper of this series (referred to as Part I [4]).

In this third and last paper we present a thorough investigation of the responsible ferromagnetic sites by means of SQUID's (Sect. 2). We have measured size and (if possible) location of their remanent magnetic moments and determined their hysteresis curve. The latter characterizes them as magnetite particles (Fe_3O_4). Starting from a formula presented in [2] we then proceed to an analysis of ^{3}He relaxation by such small magnetized particles in the weak collision limit (Sect. 3). Here the perturbing action of a particle during a close diffusion passage through its dipole field is still weak, such that the chance of depolarisation remains distinctly below 1. Putting all pieces together — including the measured pressure dependence — we can then get a fairly good estimate of the size and number of these particles. We then turn to the strong collision limit characterized by total depolarisation during a

[a] This paper comprises part of the doctoral thesis of Jörg Schmiedeskamp; *present address*: Max-Planck-Institut für Polymerforschung, 55128 Mainz, Germany.
[b] e-mail: wheil@mail.uni-mainz.de
[c] e-mail: ernst.otten@uni-mainz.de
[d] On leave from PNPI, Gatchina.

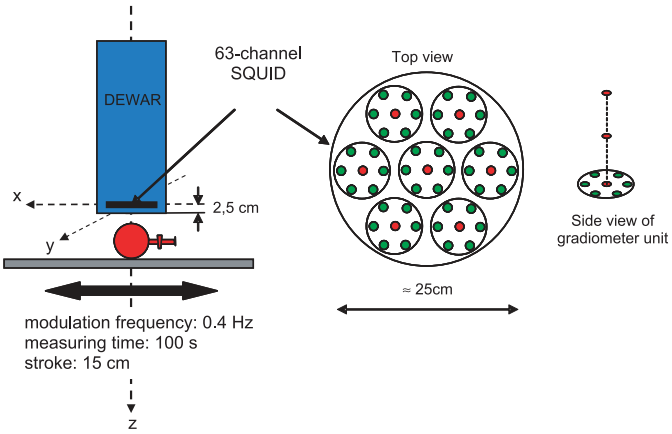

Fig. 1. Sketch of the gradiometer array to draw up a (gradient) field map of the source (here: ferromagnetic particles in a glass sample) in the (x, y)-plane of the sensors.

close encounter (Sect. 4). It is met in our cells at pressures above 1 bar. By an analytic diffusion model we find here a linear increase of the relaxation time with pressure — opposite to the case of the weak collision limit. A quantitative numerical result of relaxation by magnetized particles is obtained by a Monte Carlo simulation of the perturbing action of the dipole field on the diffusing atoms. The results of these calculations have been checked experimentally by putting a small iron piece of known size and magnetization inside a ^{3}He cell and measuring its effect on the relaxation time.

2 SQUID measurements of remanent magnetism in glass cells

In order to learn more about the size, the distribution, and the hysteresis of the remanently magnetized particles in our ^{3}He storage cells, we have performed measurements with two multi-channel SQUID systems in magnetically shielded rooms at the Physikalisch-Technische Bundesanstalt (PTB) in Berlin.

2.1 Size and distribution of remanent magnetism

The first group of measurements was performed with the 63-channel SQUID-system which is used in routine operation to record injury-related bio-magnetic fields of patients [5]. The whole setup operates inside a standard shielded room (AK3b Vakuumschmelze). By means of a mechanical modulation device the source-to-detector distance is periodically varied at 0.4 Hz along the x-axis and a lock-in technique is applied to reduce the noise level. In order to minimize the influence of global magnetic field changes the SQUID array is operated in a gradiometer configuration (see Fig. 1). It consists of 7 units, each of which comprises 7 SQUID's in the (x, y)-plane (bottom plane) measuring the field distribution therein and two more along the z-axis, measuring the z-gradient. The oscillating field values $B_k(t_i)$ (k: channel) are converted to correlation field amplitudes A_k according to

$$A_k = \sqrt{2}\frac{1}{N}\frac{\sum_{i=1}^{N}\left(B_k(t_i)-\overline{B_k}\right)\left(U\left(t_i\right)-\overline{U}\right)}{\sqrt{(1/N)\sum_{i=1}^{N}\left(U\left(t_i\right)-\overline{U}\right)^2}}. \quad (1)$$

Here $U(t_i)$ is the actual source position recorded at the digitized time intervals t_i, $(i = 1, \ldots, N)$ over which equation (1) is integrated for a total measuring time of 100 s; $\bar{U}$ is the time averaged position.

The instrument allows measurements of field pattern with a resolution of $\Delta B = 30$ fT. Theoretical correlation field-amplitudes can be generated for an analytical model of the magnetic field source and then be fitted to the measured values. As a first approach a single magnetic point dipole was chosen. As a consequence of this restriction fits of the near field of distributed magnetic sources do converge poorly resulting in increased χ^2 values.

From our GE 180 glass melt two glass flasks (GE #26 and GE #30, see Fig. 6 in Part I) were analysed along with some melt probes which were just dropped into some form. GE #26 was known to show a strong T_1 hysteresis with $T_{1max} \approx 115$ h if demagnetized and $T_{1min} \approx 3$ h if magnetized. The magnetized cell was fixed on the mechanical modulation device with 1 cm as closest approach to the bottom of the Dewar, i.e., $z_0 = 3.5$ cm with respect to the plane of the 49 gradiometer array (see Fig. 1). Four independent measurements were performed. Each time the cell was rotated clockwise around the z-axis in steps of 90°. The respective magnetic field maps are shown in Figure 2. They are well described by a single magnetic dipole whose position rotates at constant $z = (4.15 \pm 0.13)$ cm around a circle of diameter $\Phi = (5.29 \pm 0.13)$ cm in the (x, y)-plane with the centre at $x = (-0.98 \pm 0.14)$ cm, $y = (-2.2 \pm 0.1$ (x, y)-plane with the centre at $x = (-0.98 \pm 0.14)$ cm, $y = (-2.2 \pm 0.15)$ cm for the 0° position. These coordinates fit well to a point source located in or on the glass wall. In Figure 2 position and orientation of the corresponding magnetic moment in the (x, y)-plane are plotted too, showing its rotation in steps of 90°. The magnitude of the total magnetic moment, possibly integrated over a cluster of individual ferromagnetic particles, turned out to be m_{tot}(GE #26) $= (3.28 \pm 0.15)$ nA m^2. As a result we could definitely localize a ferromagnetic spot (or agglomeration of dust-like ferromagnetic particles e.g.) in or on the wall of the glass flask.

By means of a small, commercial magnetic tape demagnetizer the vicinity of this ferromagnetic site was then demagnetized and its residual field re-measured. The fit yielded the same position and orientation of the dipole but reduced in size by about a factor of 3 (m_{tot}(GE #26) $\sim$ 1.2 nA m^2).

GE #30 showed an initial $T_1 \approx 100$ h and had never been exposed to a strong magnetizing field before being measured by the SQUID-device. In contrast to GE #26 the parameter fit did not converge well towards a dipole

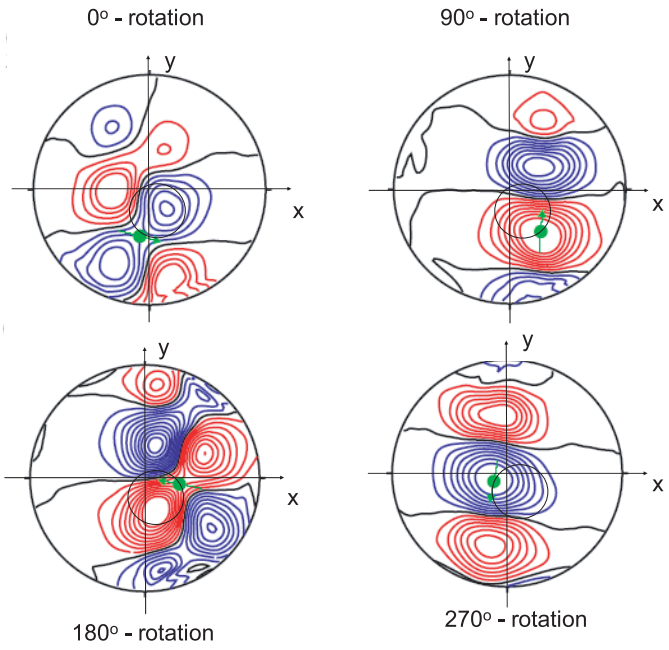

Fig. 2. Contour plot of the correlation field-amplitudes in the plane of the 49 SQUID sensor gradiometers emerging from a localized magnetic dipole (arrow) which rotates in steps of 90° around the vertical z-axis. Field steps for 0°, 90°, and 270° rotation: $\Delta B = 200$ fT, and for 180°: $\Delta B = 100$ fT, respectively.

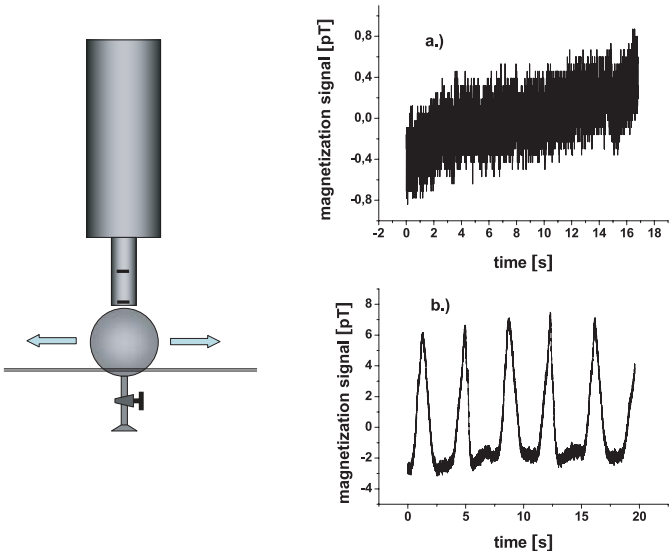

Fig. 3. Sketch of the SQUID gradiometer installed in the cooling finger of a liquid He-Dewar. The glass cell below is periodically passing the sensor: (a) recorded signal from a demagnetized cell; GE #31; (b) corresponding signal after full magnetization at $B = 3$ T.

field. Apparently several ferromagnetic sites or clusters are distributed over the cell walls at distances comparable to that of the sample to the SQUID-array. In this case the assumed single dipole-model of the source is no longer valid. The only qualitative information which could be extracted from the measured field maps was a relative increase of the field strength by about 60% after the cell had been magnetized in a field of 4.7 T. Note that for this cell we observed a ratio $T_{1,max}/T_{1,min} = 7$ between demagnetized and magnetized status.

In one of the melt probes from GE180 ($\approx 4\times3\times1$ cm^3) which was magnetized before its field pattern was measured we found a very strong single magnetic dipole with a moment of about 300 nA m^2. We shattered the probe into pieces and finally could localize the ferromagnetic site in one small fragment. Probably it had been picked up from the melt form. After demagnetization the residual moment was only 2 nA m^2. For GE #26 we located a magnetic dipole with a moment as large as 4 μA m^2 in the plastic nut which fixes the stopcock. The nut had to be removed, before the cell itself could be measured properly. Hence we found that remanently magnetized ferromagnetic contaminations may be found everywhere, an experience well-known to the experts dealing with very low magnetic fields.

2.2 Hysteresis of remanent magnetism

The hysteresis of a ferromagnet is characterized by the magnetizing field H_s, which leads to the saturation magnetization $M_s = B_s/\mu_0$, the remanence B_r, and the coercive force H_c (or B_c) which annuls the remanent magnetization. It is well-known that for a polycrystalline sample these quantities strongly depend on the domain state of the sample which in turn is a function of the grain size. Domain states change from superparamagnetic, to single domain, and finally to multidomain with increasing grain size. Furthermore, the critical grain size for domain-transitions depends on composition, temperature, and microstructure. The maximum coercive force and remanent magnetization for a given material occurs within its single domain range. For larger grain sizes, both coercivity and remanent magnetization decrease as the grain subdivides into domains. Going to smaller grain sizes, coercivity and remanent magnetization again decrease, but this time due to the randomizing effects of thermal energy. Fe_3O_4 (magnetite) is the most probable ferromagnetic contamination in or on glass surfaces and one of the most extensively studied magnetic minerals. Its grain size dependent hysteresis parameters are well-known. This will help to analyse number and average size of ferromagnetic sites in our glass vessels from measurements of remanent magnetization curves and T_1 hysteresis as well as of total remanent magnetic moments of the sites and pressure dependence of T_1.

At the PTB the hysteresis of the ferromagnetic sites in our glass vessels was measured inside a 6 layer μ-metal shielded room ($2.2 \times 2.2 \times 2.3$) m^3 with residual static magnetic field of about 2 nT [6]. A one-channel SQUID gradiometer was used to detect the magnetic signal from the glass cells which were periodically moved forth and back closely below the gradiometer. In order to reproduce the relative distances between source and sensor the cells were moved along two horizontal PVC rails (Fig. 3).

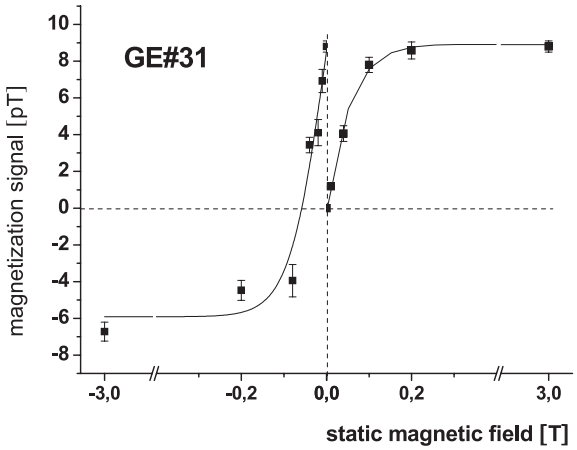

Fig. 4. Hysteresis of the remanent magnetization in the cell GE #31. For $B > 0$ the virgin curve is shown; for $B < 0$ first demagnetization is observed, followed by a reversed remagnetization.

The signals of two flasks from GE180 glass (GE #26 and GE #31, Fig. 6 in Part I) were measured first in the demagnetized state. Then the cells were put into the stray field of 10 mT of a NMR-tomograph for about 10 min which was located in the building next door. Brought back again to the SQUID-device their respective magnetization signals were re-measured. This procedure was repeated, while increasing the magnetic field step by step by placing the cells closer to the bore of the magnet, finally reaching the maximum field strength of 3 T. Care was taken in that the cells were moved in and out always in the same orientation relative to the field axis. After exposure to the 3 T field, at full magnetization, this orientation was inverted and the series of measurements repeated, starting again at the lowest field of 10 mT. Graphs (a) and (b) in Figure 3 show the gradiometer signals of the demagnetized and fully magnetized cell GE #31. While the signal amplitude remains below noise level in the former case, it reaches 8 pT in the latter. Similar signals were found for the other cell, except that still a small signal of about 0.8 pT could be traced in the "demagnetized" state. This shows that our demagnetization procedure is not optimal yet.

Plotting the signal as function of the applied magnetizing field, we obtain hysteresis curves of the remanent magnetization, shown in Figure 4 for the case of cell GE #31. Saturation is reached at a magnetizing induction of about 0.2 T (corresponding to $H_s \approx 160000$ A/m). After field reversal it is annulled at about –0.06 T (corresponding to a remanent coercive force of $H_{rc} \approx -50000$ A/m). The solid lines curves are exponential fits used as guide for the eye. For the other cell (GE #26) we get somewhat lower values ($B_{cr} \approx -0.04$ T, $H_s \approx 0.15$ T/μ_0). In order to investigate the remanent magnetization of the Pyrex part of our cells, we measured the magnetic signal arising from the stopcock and flange of cell GE #31 which had been rotated before by 180° in order to point upwards towards the SQUID sensor (compare Fig. 3). From a similar hysteresis curve of remanent magnetization we could extract the values $B_{cr} \approx -0.025$ T for the remanent coercive force and $H_s \approx 0.12$ T/μ_0 for the magnetizing field.

The grain-size dependence of remanence coercivity in magnetite is given, e.g. in reference [7], showing experimental data from crushed grains in the range of grain diameter 0.2 μm $\leq 2R \leq$ 100 μm which can be parameterized by a double-exponential fit

$$B_{cr} \cong 15.4 + 16.7 \exp(-R/(30.9\ \mu\text{m})) + 25.5 \exp(-R/(2.29\ \mu\text{m}))\ \text{mT}. \quad (2)$$

Using equation (2) our results on the remanent coercive force of 25 mT $\leq B_{cr} \leq$ 60 mT indicate grain sizes in the range 0.3 μm $\leq R \leq$ 10 μm.

3 Mechanism and analysis of ^{3}He relaxation by magnetized particles in the weak collision limit

In reference [2] an estimation of the ^{3}He relaxation due to a large number N_s of microscopically small, magnetized particles with magnetic moment m is given based on equation (1) in Part I yielding a relaxation rate $1/T_1' \approx (\mu_0/4\pi)^2 \gamma_{\text{He}}^2 (m^2/R^6) J(\tau)$. This equation is derived in the so-called weak-collision limit, where the interaction time τ of a ^{3}He-atom with a particular m is assumed to be much shorter than the Larmor period $2\pi/\omega_1$ of spin precession around the perturbing field, that is, if $\omega_1 \tau \ll 1$. With ω_0 being the ^{3}He Larmor frequency in the external magnetic field (unperturbed field) the spectral density $J(\tau) = \tau/(1+\omega_0^2\tau^2)$ reduces to $J(\tau) \approx \tau \approx R^2/6D$ in case of $\omega_0 \tau \ll 1$ where D is the diffusion constant of ^{3}He. At room temperature and gas pressure p, the diffusion constant amounts to $D = 1.84 \times 10^{-4}$ (m^2 bar/s)/p [8]. After having factorized in the fraction of ^{3}He spins interacting with the sites Jacob et al. obtain the relaxation rate

$$\frac{1}{T_1} \approx \left(\left(\frac{\mu_0}{4\pi} \right)^2 \frac{\gamma_{\text{He}}^2 m^2}{R^6} \tau \right) \frac{2\pi R^3}{3V} N_S = \left(\frac{\mu_0}{4\pi} \right)^2 \frac{N_S \pi \gamma_{\text{He}}^2 m^2}{9RV\, 1.84 \times 10^{-4}}\, p. \quad (3)$$

In this derivation the assumption is made that the N_S sites are located on the surface with their effective interaction volume V_{int} given by half spheres of radius R, where R is the characteristic particle radius[1]. Characteristic for the weak collision limit with the condition $\omega_0 \tau \ll 1$ is the linear dependence of the relaxation rate on the pressure p and its quadratic dependence on the magnetization m of the particles. In the strong collision case ($\omega_1 \tau \gg 1$),

[1] Since the ^{3}He atoms apparently do not enter the magnetized particle one may argue, whether one should define instead the interaction volume between R and $2R$, for instance, and replace the three dimensional diffusion length R by a one dimensional of $2R$ for entering and leaving the hollow half sphere in radial direction. One then looses a factor of 8 in the mean squared interaction field $\langle B_{int}^2 \rangle$ and gains back equivalent factors 4/3 in τ and 7 in V_{int}.

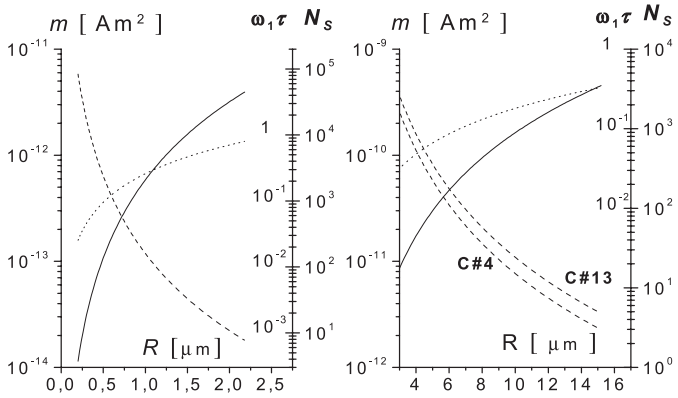

Fig. 5. As function of the particle radius are plotted: (i) remanent magnetic moment m (full lines), (ii) precession angle within the dipole field $\omega_1\tau$ at a pressure of 8 bar (left) and 0.2 bar (right) (dotted lines), (iii) number of particles N_s (dashed lines) as calculated from the results of reference [2] (left) and cells C #4 and C #13 (right).

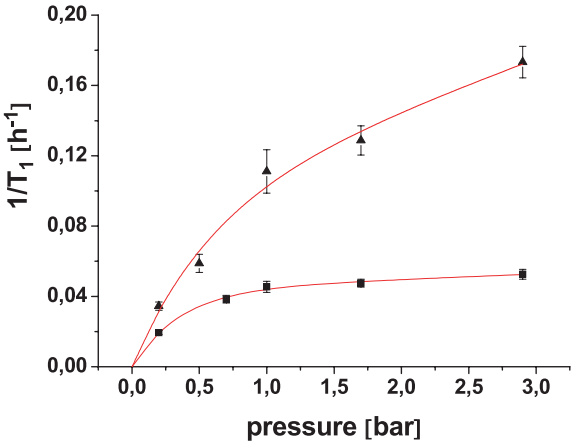

Fig. 6. Measured relaxation rates in magnetized glass flasks C #4 (squares) and C #13 (triangles) from Corning 1720 as function of ^{3}He gas pressure. The roughly linear increase below 1 bar (according to the weak collision theory) levels off towards higher pressure values.

where equation (3) is no more valid, the relaxation rate will scale with $1/p$ and depend almost linearly on m (see Sect. 4). From equation (3) we obtain a relation between the number N_S, the magnetic moment m, and the radius R of the particles on one hand side and experimentally accessible quantities on the other side:

$$\frac{N_S m^2}{R} = 0.127 \times 10^{-5} (\mathrm{A^2\,s\,bar}) \mathrm{V} \frac{1/T_1}{p}. \qquad (4)$$

We can interpret these results in more detail if we assume the particles to be magnetite. Its bulk saturation magnetization is $M_s = 4.69 \times 10^5$ A/m [7], corresponding to $3.75\mu_B$ per formula unit. The remanent moment of magnetite particles with the radius R is then

$$m = (4\pi/3) R^3 M_s \left[1.3 \times 10^{-4} (R/\mathrm{m})^{-0.555}\right]. \qquad (5)$$

Here the term in square brackets fits in the range 10^{-7} m $\leq R \leq 10^{-3}$ m to the empirical R-dependence of the ratio of remanent to saturated magnetization (M_r/M_s) [7] (see Fig. 5). Inserting equation (5) into equation (4) we get in addition the dependence of N_s on R for a particular cell, which is also plotted in Figure 5. Furthermore, with the help of equation (5) we can check the weak collision limit $\omega_1\tau \approx \omega_1 R^2/6D \ll 1$ (as a first estimate this relation is valid to the limit ≤ 1). For low B_0 the total field within the interaction zone is dominated by the local moment m, leading to the estimate

$$\omega_1 \approx \gamma_{\mathrm{He}} \mu_0 m/((4/3)\pi R^3) = \gamma_{\mathrm{He}} \mu_0 M_r. \qquad (6)$$

In Figure 5 the resulting R-dependence of $\omega_1\tau$ is plotted, too, for $p = 8$ bar in the left plot and for 0.2 bar in the right hand-side plot. Since the authors of reference [2] have observed a perfectly linear increase of $1/T_1$ up to 8 bar in their cell, we may conclude the weak collision limit to be well obeyed in their case, say $\omega_1\tau \leq 0.1$. This would correspond to a particle radius $R \leq 0.5$ μm and a moment of $m \leq 0.1$ pA m^2 according to Figure 5 (left). One may now insert the slope of $(1/T_1)/p = 3.11 \times 10^{-3}$ h^{-1}/bar reported in reference [2] for a cell of volume $V = 50$ cm^3, into equation (4), as well as the above limits and extract a lower limit for the particle number of $N_s \geq 2700$ (Fig. 5, left plot). The total moment in this limit amounts to $m_{tot} = N_s m \approx 0.3$ nA m^2 which is close to the values measured in our cells by SQUID-gradiometry (Sect. 2). The SQUID measurements cannot discriminate, however, between a single, concentrated and a distributed, dust-like dipole source within its spatial resolution of a couple of cm. The authors of reference [2] arrive at similar numbers starting from the assumption that the particles consist of metallic iron with a (constant) magnetization of $1\mu_B$ per iron atom.

In order to check whether the ferromagnetic contamination in our uncoated aluminosilicate glass flasks consists also of dust-like particles or of single macroscopic particles, we measured the relaxation rate of two Corning 1720 glass cells 1.1 l volume (C #4 and C #13 in Fig. 6 in Part I) as function of the gas pressure. (In the demagnetized state they reach relaxation times T_{1max} of 190 h and 100 h, respectively.) The cells were magnetized prior to the relaxation measurements. The results are shown in Figure 6. *Grosso modo*, we see a roughly linear increase of the relaxation rate with pressure below 1 bar indicating that the relaxation occurred on microscopic dust-like particles obeying the weak collision limit. $1/T_1$ levels off at higher pressures. This observation is attributed to the beginning of the strong collision limit with $\omega_1\tau \geq 1$. The crossover between the two regimes, defined by $\omega_1\tau = 1$, seems to occur around $p \approx 0.7$ bar for cell C #4 and around $p \approx 1$ bar for cell C #13 (see Fig. 6). On the right ($\omega_1\tau$)-plot of Figure 5 we find this point at radii of R(C #4) $\approx$ 13 μm and R(C #13) $\approx$ 10 μm, respectively (properly scaled with $p/(0.2$ bar)). These radii compare well with those derived from the measured coercive forces via equation (2). The corresponding

magnetic moments are $m(\mathrm{C}\ \#4) \approx 2.9 \times 10^{-10}$ Am^2 and $m(\mathrm{C}\ \#13) \approx 1.5 \times 10^{-10}$ A m^2, respectively.

In addition, we derive the number of particles via equation (4) from the initial slopes of the relaxation curves in Figure 6, which we find to be $(1/T_1 p)_{\mathrm{C}\#4} \approx 0.07$ h^{-1}bar^{-1} and $(1/T_1 p)_{\mathrm{C}\#13} \approx 0.12$ h^{-1}bar^{-1}, respectively. These slopes give $N_s(\mathrm{C}\ \#4) \approx 4$ and $N_s(\mathrm{C}\ \#13) \approx 21$. The corresponding total moments are calculated to $m_{tot}(\mathrm{C}\ \#4) \approx 1.2$ nA m^2 and $m_{tot}(\mathrm{C}\ \#13) \approx 3$ nA m^2, respectively. For comparison, we quote again the directly measured value of 3.28 nA m^2 obtained for cell GE #26 by the SQUID-gradiometry measurements.

Altogether we have obtained a very consistent picture of the quantity of the ferromagnetic contamination in our cells and their relaxing action on the ^{3}He-spins: the coercive force as well as the pressure at which the transition from the weak to the strong collision limit occurs, point to magnetite particles of radius $R \approx 10$ μm with remanent magnetic moments of order $m = O(10^{-10}\mathrm{Am}^2)$. The initial slope at which the relaxation rate rises with pressure as well as the total remanent moment $m_{tot} = O$ (nA m^2) enable us to estimate the number of particles to be of the order of 10. Moreover, we conclude that the magnetite particles are essentially located on the surface of the glass cells. A homogeneous distribution within the glass wall would require a 100 times larger number of particles, since their interaction radius is only of the order of their size, i.e. 10 μm. In the molten state of glass such particles cannot exist under any circumstances. However, during the process of thermoforming at corresponding lower temperatures and relatively long intermediate time intervals reduction of hematite to magnetite may set in; and due to surface germs surfaces have the tendency to crystallization in particular. On the other hand, we did not observe a clear-cut correlation between number/size of magnetite particles and the intrinsic iron content of the melt. Hence we have to consider surface contaminations due to tools used during the process of glass blowing. So far we did not investigate yet at which stage such contamination might have been brought in. One may ask why these particles have not been washed out during the cleaning process of the cells ahead of evacuation: during blowing they might have sunken into the glass surface and been wetted by a microscopic glass layer. In this case only rigorous etching would have removed them. In any case, we have observed much bigger and much less ferromagnetic particles in our cells than the authors of reference [2] in their samples. This points to a different source in reference [2], possibly the Rb filling as suggested there.

4 Relaxation in the strong collision limit

The foregoing analysis has shown that the weak collision limit of ^{3}He relaxation by magnetized particles of radius 10 μm, observed in our cells, starts to turn over into the strong collision limit ($\omega_1 \tau > 1$) at pressures $p \geq 1$ bar. Since we are filling these cells routinely up to 3 bar for shipping and up to 6 bar as targets, we are definitely entering this regime and have tried, therefore, to get some insight into it by theory and experiment. Qualitatively, one could argue that the dipole on the wall creates a certain volume, say a half sphere of radius R_r around itself within which the nuclear polarization fully relaxes due to a random precession angle $\omega_1 \tau \gg 1$ in the perturbing dipole field. The loss of polarized atoms $N\langle \dot{P} \rangle$ would then equal the diffusion current I_P of polarized atoms into that half sphere. Let us consider a polarization of degree P_1 at some radius $R_1 \gg R_r$. By solving the diffusion equation of the current density $\boldsymbol{j}_P = -D\ \mathbf{grad}(P\, d\mathrm{N}/dV)$ within the surrounding half-sphere one finds a diffusion current of

$$I_P = \frac{4\pi D(N/V)P_1}{R_1^{-1} - R_r^{-1}} \approx -4\pi D(N/V)P_1 R_r. \qquad (7)$$

Equation (7) implies a steep hyperbolic decrease of $P(r)$ in the diffusion zone. Therefore, it is sufficient to consider a very small zone of negligible volume (V_1) as compared to that of the cell (V) and to set $P(r > R_1) = P_1 = \langle P \rangle$. The relaxation rate then follows to be

$$1/T_1 = -\langle \dot{P}/P \rangle \approx 4\pi D R_r/V. \qquad (8)$$

Here the diffusion coefficient introduces the expected decrease $1/T_1 \sim 1/p$ or simply $T_1 \sim p$. The weak point of this derivation is the ad hoc ansatz of a pressure independent "black hole" radius R_r, however.

A quantitative analytic solution of the strong collision problem is not known to us. We have aimed at a numerical solution, therefore, by simulating diffusion and relaxation within a magnetic dipole field by Monte Carlo methods (MC). To that end we integrate the Bloch equations along diffusion random walks, applying a code which has been published by part of us in an earlier paper on a similar problem reference [9]. The magnetic field under study is the superposition of a magnetic dipole field $\boldsymbol{B}_D$ and a homogeneous field $\boldsymbol{B}_0$ given by

$$\boldsymbol{B}(r) = \boldsymbol{B}_D + \boldsymbol{B}_0 = \frac{\mu_0}{4\pi} \frac{3\hat{\boldsymbol{r}}(\hat{\boldsymbol{r}} \cdot \boldsymbol{m}_p) - \boldsymbol{m}_p}{|r|^3} + \boldsymbol{B}_0. \qquad (9)$$

In the following a point like magnetic moment $\boldsymbol{m}_p$ is assumed to be embedded in the wall of the glass at a distance $\boldsymbol{d}$ from its surface (see Fig. 7a). We confine the discussion to the cases that $\boldsymbol{m}_p$ points along the z-axis, parallel to the surface and that the external field $\boldsymbol{B}_0$ is parallel or anti-parallel to the moment. Assuming $m_p = 400$ nA m^2, $B_0 = 1$ mT, and $d = 50$ μm, the amount of the resulting field $|\boldsymbol{B}_D + \boldsymbol{B}_0|$ inside the gas volume is plotted in Figures 7b and 7c as function of cylindrical co-ordinates z and r with respect to the dipole for the two cases $\boldsymbol{B}_0 \uparrow\uparrow \boldsymbol{m}_p$ and $\boldsymbol{B}_0 \uparrow\downarrow \boldsymbol{m}_p$, respectively. Two features should be emphasized: (i) there are strong magnetic field gradients at short distances from the dipole; (ii) the absolute field shows a zero crossing for the parallel case at $z \approx 0$ mm and $r \approx 0.35$ mm and for the anti-parallel case at $z \approx 0.5$ mm and $r \approx 0$ mm, respectively. Thus we expect strong relaxation of polarized ^{3}He atoms diffusing through these particular regions. Position, shape, and spatial extension of zero crossings depend not only on the size but also on

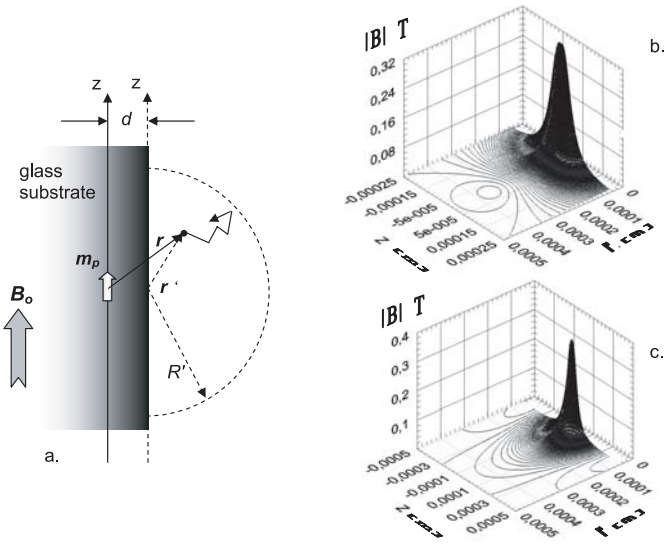

Fig. 7. (a) Magnetized particle at distance d beneath the glass surface whose point like magnetic moment $\mathbf{m}_p$ is pointing along the z-axis parallel to the surface. r = position vector of a diffusing ^{3}He atom. $\boldsymbol{B}_0$ = external magnetic field. (b) Plot of resulting field amount $|\boldsymbol{B}_D + \boldsymbol{B}_0|$ as function of z and r for $m_p = 400$ nAm^2, $B_0 = 1$ mT, and $\boldsymbol{B}_0 \uparrow\uparrow \boldsymbol{m}_p$. (c) Corresponding plot with $\boldsymbol{B}_0 \downarrow\uparrow \boldsymbol{m}_p$.

the relative orientation of $\boldsymbol{B}_0$ and $\boldsymbol{m}_p$. This may cause an orientation dependence of ^{3}He relaxation, as has indeed been observed recently in SEOP cells [3]. The relaxation depends strongly on the distance d of the dipole from the surface. According to Figures 7b and 7c we may expect almost no effect any more for $d \geq 0.4$ mm, even for this rather large moment (a factor of 100 over those discussed above).

In order to save computer time we speed up relaxation by choosing relatively large moments and studied diffusion only in a restricted hemisphere of volume $V' = (2\pi/3)(R')^3$ (see Fig. 7a). In order to avoid boundary effects we define a criterion for the appropriate size of V', namely, that for volumes $\tilde{V}' \geq V'$ the corresponding relaxation time should scale as $\tilde{T}_1' = T_1'(\tilde{V}'/V')$ in the MC simulation. For the field parameters chosen we could restrict R' to 0.5 mm. The dipole induced relaxation time in a cell of volume $V \geq V'$ is then given by

$$T_1 = T_1'(V/V'). \tag{10}$$

^{3}He diffusion is simulated for a Maxwellian velocity distribution at $T = 300$ K. Starting at a random position inside V' the trajectory of the particle undergoing gas-kinetic collisions is tracked using $P(\lambda)d\lambda = (1/\lambda_0)\exp(-\lambda/\lambda_0)d\lambda$ as probability distribution of the mean free path length λ_0. At $p = 1$ bar the mean free path length λ_0 is about 50 nm. An analytical expression for the double differential scattering cross-section $(d^2\sigma/d\,\vartheta dE)$ (with ϑ = scattering angle, E = centre of mass energy) is given in reference [10]. It is strongly forward peaked. As a first check we reproduced the value of the free diffusion coefficient D of ^{3}He at 1 bar to be $D \approx 2$ cm^2/s [8]. Note, that λ_0 should not be mixed up with the much longer mean free path $\bar{\lambda}$ entering the usual diffusion equation $D = (1/3)\bar{v}\bar{\lambda}$, where $\bar{\lambda}$ is defined via $\bar{\sigma} = 1/n\bar{\lambda} = \int_{\vartheta,E}(d^2\sigma/d\,\vartheta dE)(1 - \cos\,\vartheta)d\vartheta dE$ (with n = particle density); $\bar{\lambda}$ is equivalent to the geometric cross-section of a hard sphere.

The Bloch equations were integrated using standard Runge-Kutta numerical integration schemes with time intervals of $\delta t = 1$ ns during which the magnetic field vector was kept constant. The accuracy of this discretisation was checked using different time steps. Within V' the atoms were assumed to be initially fully polarized, i.e., $P_0 = 1$. As a result from space tracking of 2000, homogeneously distributed atoms, the average polarization $\langle P(t_k)\rangle$ was determined at times $t_k = k\Delta t$ with $\Delta t \gg \delta t$ and $k = 1, 2, ..., K$. The simulation was stopped at $\langle P(t_k)\rangle \cong 1/e$. The corresponding relaxation time was found to be of order $T_{1s} \sim O(\text{ms})$.

In order to identify the main sources of relaxation the relative field gradient $|\nabla B|/B = \sqrt{(\partial B/\partial z)^2 + (\partial B/\partial r)^2}/B$ is calculated for the field distributions shown in Figures 7b and 7c (cylindrical symmetry). The results are plotted in Figures 8a and 8b as function of z and r for both orientations of the magnetic guiding field. As a measure of spin relaxation we define an angular velocity $\omega_s = |d(\arccos(\boldsymbol{I}\cdot\boldsymbol{B}/IB))/dt|$ at which the angle of projection of nuclear spins $\boldsymbol{I}$ onto the respective field axis $\boldsymbol{B}(r)$ changes. This is displayed in Figures 8c and 8d. One recognizes immediately the strong correlation between the spin relaxation rate and the strength of the relative magnetic field gradient. Both show sharp maxima at the positions of the field zero crossings and at very short distance from the dipole.

The ^{3}He relaxation rates, resulting from the MC-simulations of the atomic diffusion within a restricted hemisphere of radius $R' = 0.5$ mm for some characteristic values of the relevant parameters m_p, d, B_0, and p are plotted in Figures 9a to 9d. The increase of relaxation rate with growing moment is shown in Figure 9a for several distances d from the surface with all other parameters fixed. Asymptotically it appears to be linear, whereas the contribution of the cut off d levels off. Figure 9b shows the expected fast decrease of the relaxation rate with the distance from the surface for a moment of 100 nAm^2. Beyond 0.3 mm the relaxation has practically vanished. For the 1000 times smaller moments, which are actually observed in our vessels, this would of course already occur at much smaller distances; but we refrained from MC simulations of the correspondingly much longer relaxation times. Quite interesting is the quasi-hyperbolic dependence of the relaxation rate on B_0 shown in Figure 9c. The steep increase towards low field is due to the rapid expansion in radius and volume of the strongly relaxing zones around the dipole and in particular around the zero field crossing. The pressure dependence in Figure 9d shows the linear relation $T_1' \sim p$ above 0.2 bar as expected from the analytic diffusion model already; the slope is 0.19×10^{-6} h/bar.

For a qualitative experimental confirmation of the field dependence of ^{3}He relaxation in magnetized cells, cell

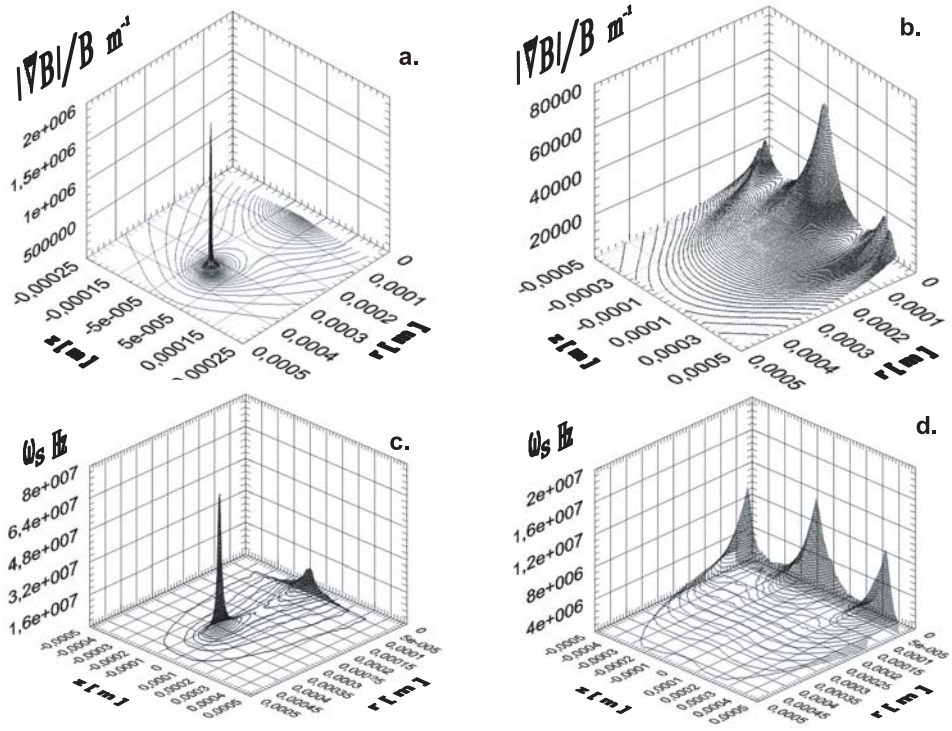

Fig. 8. Correlation between relative magnetic field gradient $|\nabla B|/B$ and spin relaxation rate ω_s for $\boldsymbol{B}_0 \uparrow\uparrow \hat{\boldsymbol{z}}$ (a) and (c) and $\boldsymbol{B}_0 \uparrow\downarrow \hat{\boldsymbol{z}}$ (b) and (d), plotted in the (r, z)-plane. Distance of point dipole of size 400 nA m^2 from the surface: $d = 0.05$ mm.

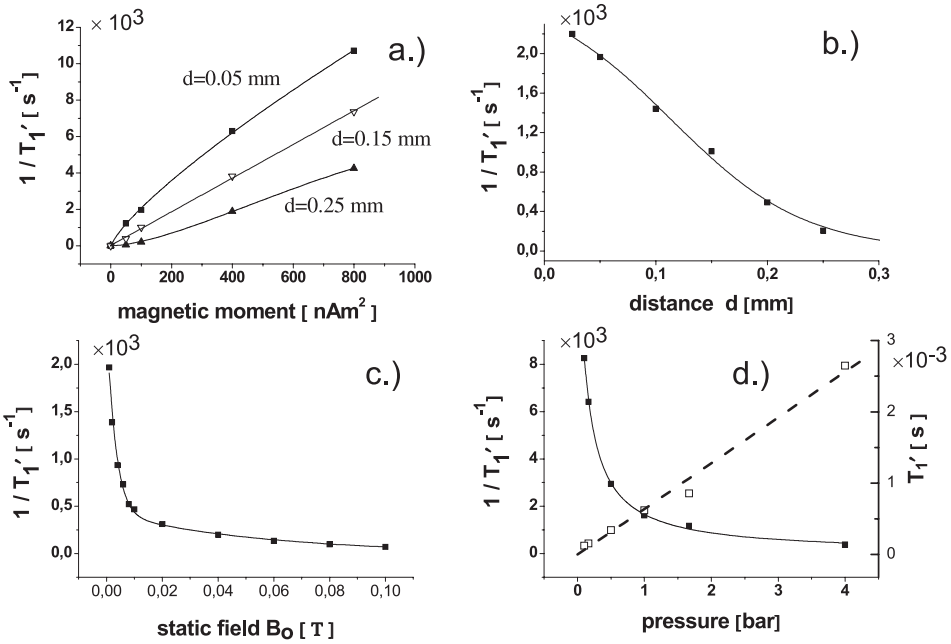

Fig. 9. MC simulation of the relaxation rates $1/T_1'$ of polarized ^{3}He diffusing at room temperature within a hemisphere of volume $V' = (2\pi/3)(R')^3 = 0.262 \times 10^{-9}$ m^3. (a) $1/T_1'$ plotted as a function of magnetic moment for three different distances d of the point-like dipole from the glass surface ($\boldsymbol{B}_0 \uparrow\uparrow \hat{\boldsymbol{z}}$, $B_0 = 1$ mT, $p = 1$ bar), (b) as a function of d ($m_p = 100$ nA m^2, $\boldsymbol{B}_0 \uparrow\uparrow \hat{\boldsymbol{z}}$, $B_0 = 1$ mT, $p = 1$ bar), (c) as function of B_0-field ($m_p = 100$ nA m^2, $\boldsymbol{B}_0 \uparrow\uparrow \hat{\boldsymbol{z}}$, $d = 0.05$ mm, $p = 1$ bar), (d) as function of the p ($m_p = 100$ nA m^2, $\boldsymbol{B}_0 \uparrow\uparrow \hat{\boldsymbol{z}}$, $B_0 = 1$ mT, $d = 0.05$ mm). In (d) a plot of T_1 is added (dashed line) in order to show the (approximate) linearity with p. The lines are fitting the points in order to guide the eye.

GE #26 was magnetized to saturation in the 1.5 T field of a MR scanner. The relaxation time with the high field applied was measured to be $T_1 = (30 \pm 2.5)$ h. Subsequently the relaxation time was re-measured at low field ($B_0 \approx 0.8$ mT) giving $T_1 = (3 \pm 0.3)$ h. Care was taken that the direction of the remanent magnetization was kept parallel to B_0 also in the case of low field. Although the saturated magnetization exceeds the remanent one by a factor of 13 for magnetite particles of radius 10 μm (see Eq. (5)), the relaxation time was found to be 10 times longer in the high field. Indeed, in the strong collision limit our MC simulation predicts a fast drop of relaxation rates at high fields (Fig. 9c). This gives us at least a qualitative understanding of the observed increase of T_1. Note that the parameters of our MC simulations do not fit to the low collision limit, whereas the low field measurement probably does.

In order to verify experimentally the functional pressure dependence we put a piece of magnetized iron with a weight of 27 μg directly into a Corning 1720 glass cell of $V \approx 0.7$ l and measured the relaxation times at three different pressures (Fig. 10). A linear fit T_1 [h] $\approx$ (0.438 h/bar)p describes the data fairly well. We have

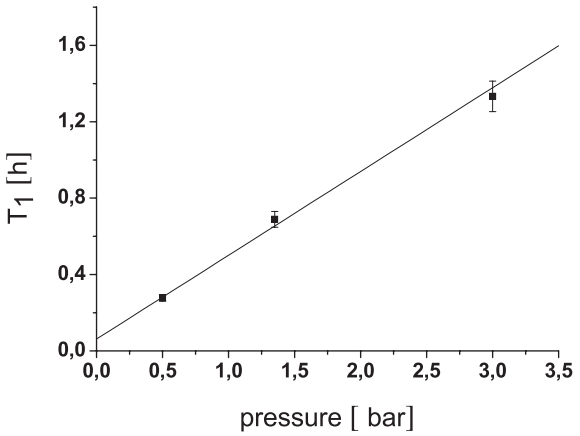

Fig. 10. Measured ^{3}He relaxation time as function of gas pressure in a Corning 1720 glass cell of volume $V = 0.7$ l, containing a small magnetized iron piece with mass of 27 μg and remanent magnetic moment of $m \approx 350$ nA m^2. A straight line fit to the data (solid line) yields T_1 [h] $= ((0.438 \pm 0.028)$ h/bar$)p + (0.062 \pm 0.025)$.

measured the hysteresis curve of this piece by means of a vibrating-sample magnetometer (described for example in Ref. [11]) and found a remanent moment of 350 nA m^2. We may insert this value into Figure 9a and read from the plot a relaxation rate of $1/T_1' \approx 3500$ s^{-1} at $d \approx 0.12$ mm. The latter value corresponds to the radius of an iron half sphere weighing 27 μg and lying *on* the glass surface. We regard this situation being fairly equivalent to a point dipole lying at the distance d *beneath* the surface as assumed in the MC simulation (see above). Scaled with the ratio of the volumes (see Eq. (10)) the MC simulation would predict at $p = 1$ bar a relaxation time of $T_1 \approx 13$ min which is a factor of 2 below the measured value. In view of the simplifications made, we regard this to be a satisfactory agreement.

We may also insert the measured slope of 0.438 h/bar into the analytic formula (8) and deduce an effective relaxation radius of $R_r = 0.17$ mm, slightly larger than the particle radius; it would encircle fairly well the strongly relaxing zones in Figure 8 which have been calculated for comparable parameters.

We have performed another measurement with the iron piece demagnetized beforehand. From the measured magnetization curve we deduce that it will be re-magnetized in the measuring field of 0.8 mT to a moment of about 60 nA m^2. The relaxation time at 1 bar was found to be $T_1 = 3.2$ h, a factor 6.3 higher than measured for the remanent moment. This is again in fair agreement with the ratio of 5.8 of the moments as is expected from the linearity $1/T_1 \sim m$ displayed in the MC simulations (Fig. 9a).

Summarizing, we find for the case of the strong collision limit satisfactory agreement between calculations and experiment in all important features.

5 Conclusions

We have observed a drastic reduction of the relaxation time in our (uncoated) cells after exposure to the strong magnetic field of a MR tomograph. Long relaxation times can be recovered by an ordinary demagnetization procedure. (Similar experience has been reported before for Rb coated cells and has been ascribed to the coating procedure.) By SQUID measurements in a magnetically shielded environment we have identified the corresponding remanent dipole moments and determined their nature (magnetite) and size ($\approx$10 μm) by measuring their hysteresis. Additional information has been obtained from measurements of the pressure dependence of the relaxation rate. Below 1 bar it rises linearly with p according to the weak collision limit which is characterized by a small change of the phase of Larmor precession ($\omega_1\tau < 1$) during the time τ of interaction with the local dipole. The slope allows us to estimate the number of particles to be $\approx$4 in one and $\approx$21 in another cell. Above 1 bar the respective curve bends over into the strong collision limit ($\omega_1\tau > 1$). This finding points again to a particle size of about 10 μm.

We have studied the non-perturbative, strong collision limit (which applies for larger moments at higher pressures) by Monte Carlo simulation of the diffusion of polarized ^{3}He spins through a dipole field added to a homogeneous one. Here a strong ("black") relaxation is concentrated in two regions of strong relative field gradients, one at very short distances from the dipole, the other in the region where the dipole field cancels the homogeneous one. In this regime the relaxation rate rises linearly with the dipole moment (as compared to a quadratic rise in the perturbative weak collision limit) and decreases with pressure like $1/p$. The latter is understood also in terms of an analytical model which calculates the diffusion current into a totally relaxing "black" zone having an effective relaxation radius R_r. We have verified our Monte Carlo simulations experimentally by measuring the relaxation induced by a small soft iron grain (27 μg) within the cell and found satisfactory quantitative agreement with all theoretical predictions.

Our prime interest in the matter presented in this series of three papers was directed towards a reproducible production of transport vessels for hyperpolarized ^{3}He gas with relaxation times of 100 h or more. This goal has been fully achieved. It turned out, however, that this task was not just a matter of developing and obeying some simple recipes. Rather it drew us into a broad field of relaxation physics of ^{3}He with more open questions and experimental complications than anticipated. By now we have gained a clearer and wider view of these relaxation phenomena experimentally as well as in terms of (partly revised, partly new) theoretical concepts which are in qualitative (partly quantitative) agreement with the experimental findings. What is still to be done? From a practical standpoint of view it would be useful, for example, to know how the ferromagnetic contaminations have sneaked into the vessels and how such surface contamination can be avoided. Further theoretical attempts could be directed towards

quantum chemical calculations of ^{3}He relaxation at dangling bonds and metal surfaces for which we present but qualitative or semi-empirical considerations.

This work was supported by the Innovationsstiftung Rheinland Pfalz under project number 539, by the Schott Glas Fonds of the company Schott AG, Mainz, and by the Deutsche Forschungsgemeinschaft in the frame of the Forschergruppe FOR 474. One of the authors (Yu. Sobolev) was supported by the Russian RFFI under grant number 03-02-17305. We are grateful to G. Jakob for determining the magnetic properties of the iron grain.

References

1. W.A. Fitzsimmons, L.L.Tankersley, G.K. Walters, Phys. Rev. **179**, 156 (1969)
2. R.E. Jacob, S.W. Morgan, B. Saam, J.C. Leawoods, Phys. Rev. Lett. **87**, 143004-1 (2001)
3. R.E. Jacob, J. Teter, B. Saam, W.C. Chen, T.R. Gentile, Phys. Rev. A **69**, 021401(R) (2004)
4. J. Schmiedeskamp, W. Heil, E.W. Otten, R.K. Kremer, A. Simon, J. Zimmer, Eur. Phys. J. D **38**, 427 (2006)
5. G. Wübberler, J. Mackert, F. Armbrust, M. Burghoff, B.M. Mackert, K.D. Wolff, J. Ramsbacher, G. Curio, L. Trahms, Appl. Supercond. **6**, 559 (1998)
6. S.N. Erné, H.D. Hahlbohm, H. Scheer, Z. Trontelj, in *Biomagentism*, edited by S.N. Erné, H.D. Hahlbohm, H. Lübbig (Walter de Gruyter, Berlin, New York, 1981), p. 79
7. C.P. Hunt, B.M. Moskowitz, S.K. Banerjee, *Rock Physics and Phase Relations, a Handbook of Physical Constants*, edited by Th.J. Ahrens (AGU Reference Shelf, 1995), Vol. 189
8. R. Barbé, M. Leduc, F. Laloë, J. Phys. (Paris) **35**, 935 (1974)
9. J.M. Pendlebury, W. Heil, Yu. Sobolev, P.G. Harris, J.D. Richardson, R.J. Baskin, D.D. Doyle, P. Geltenbort, K. Green, M.G.D. van der Grinten, P.S. Iaydjiev, S.N. Ivanov, D.J.R. May, K.F. Smith, Phys. Rev. A **70**, 032102 (2004); St. Baeßler, W. Heil, W. Kilian, V. Kirste, H. Rinneberg, F. Seifert, Yu. Sobolev, Phys. Rev. A (to be published)
10. R. Helbing, H. Pauly, Z. Phys. **179**, 16 (1964)
11. S. Foner, Rev. Sci. Instr. **30**, 548 (1959)